Photoacoustic Ultrasound for Enhanced Contrast in Dental and Periodontal Imaging

11

Colman Moore and Jesse V. Jokerst

11.1 Introduction

Ultrasound is a long-standing tool in medical diagnosis. Its benefits include affordability, high spatiotemporal resolution, sensitivity, and safety—it is ideally suited for imaging soft tissue and bone surfaces simultaneously. Despite these advantages, it is surprisingly uncommon in clinical dentistry. Nevertheless, a variety of reports have been published on oral applications of ultrasound; for an overview of the field to date, we recommend previously published reviews on this topic as well as the other chapters in this textbook [1–8]. Briefly, the scope of ultrasound applications includes visualization of dental and gingival anatomy, the detection of caries, dental fractures and cracks, gingival thickness measurements, periapical lesions, maxillofacial fractures, periodontal bony defects, muscle thickness, temporomandibular disorders, and implant dentistry [9].

Ultrasound imaging systems use piezoelectric transducers to transmit high frequency (1–50 MHz) pulses through target tissue and detect the reflected waves. Because sound waves are mechanical vibrations, the speed of sound through a particular medium depends on the acoustic impedance of the material. At interfaces between tissue types with distinct acoustic impedances, a fraction of the ultrasonic pulse is backscattered, while the other part is transmitted. The magnitude of the

C. Moore
Department of NanoEngineering, University of California San Diego, La Jolla, CA, USA
e-mail: cam081@ucsd.edu

J. V. Jokerst (✉)
Department of NanoEngineering, University of California San Diego, La Jolla, CA, USA

Materials Science and Engineering Program, University of California San Diego, La Jolla, USA
Department of Radiology, University of California San Diego, La Jolla, CA, USA
e-mail: jjokerst@ucsd.edu

reflected pulse (echo) scales with the impedance mismatch at the boundary. Therefore, the intensity of the returning echo and the time it takes to reach the transducer are the two main components used to reconstruct images. However, one of the main drawbacks of ultrasound is its limited contrast. The modality can resolve anatomical features but cannot probe molecular components of disease (nucleic acids, proteins, enzymes, etc.). Recent progress has been made in activatable ultrasound contrast agents, but these still can only boost the grayscale intensity in a given region; they cannot produce spectrally unique signal. Fortunately, photoacoustic ultrasound has emerged as a fast-growing and promising technique for augmenting conventional ultrasound with the spectral contrast of optical imaging.

Photoacoustic ultrasound harnesses the photoacoustic effect—a phenomenon first observed by Alexander Graham Bell that occurs when the energy from light is absorbed by a material and released as an acoustic vibration. For imaging, a near-infrared (NIR) light source is used to pulse photons (1–100 ns) onto an absorbing target or tissue. NIR light is used because it can propagate through tissue better than blue or green wavelengths. The tissue being irradiated by the NIR absorbs the light and experiences brief (nanosecond) thermoelastic expansion. This expansion generates broadband acoustic waves that can be detected with conventional ultrasound transducers. Importantly, there is no bulk heating of the tissue. This is because the incident laser pulse is shorter than the thermal and stress relaxation times of the target; thus, the system becomes mechanically and thermally confined and the fractional volume expansion of the target can be neglected [10]. Therefore, the initial pressure rise (i.e. the generated photoacoustic wave) is proportional to the optical fluence and absorption coefficient of the material. The resulting photoacoustic wave propagates in three dimensions and is detected by either a single element ultrasound transducer or an array of transducer elements. From here, if the fluence is assumed to be locally homogenous, an image can be reconstructed based primarily upon differences in the absorption coefficient of tissue components effectively mapping the pressure wave distribution.

A variety of hardware configurations are commonly used in research applications: These primarily include photoacoustic tomography, photoacoustic microscopy, and photoacoustic endoscopy [11]. The body possesses a number of endogenous absorbers but exogenous contrast agents can also be used. The main sources of endogenous contrast are NIR-absorbing molecules such as oxygenated and deoxygenated hemoglobin, melanin, lipids, and water [12]. These targets have often been used to image hemodynamics [13], blood oxygen saturation [14, 15], and cancers [16, 17]. However, a wide variety of exogenous contrast agents—often small molecules or nanoparticles—have also been developed to boost contrast and probe specific biomarkers or disease states [18]. From a materials perspective, the current landscape of these agents primarily consists of organic small molecules [19], inorganic nanomaterials [20, 21], and organic nanoparticles [22, 23].

The preclinical applications of photoacoustic imaging for oral health have been growing in the past decade. Early work on this topic was focused on optical and photoacoustic spectroscopic measurements of oral tissue. The induced temperature distributions of photoacoustic excitation and the absorbing/scattering behavior of incident light have also been characterized. Following this, investigations have pro-

ceeded on dental pulp characterization as well as enamel/dentin imaging for early detection of caries and cracks. Recently, the field has expanded into characterization of the periodontium via non-invasive imaging of the periodontal pocket. Here, we review the developments in oral photoacoustics to date and offer perspectives on future progress in this burgeoning field.

11.2   Optical and Photoacoustic Characterization of Oral Tissues

Early investigations into dental applications of photoacoustics largely focused on the determination of optical and photoacoustic properties of oral tissue within the optical window. In medical imaging, the optical window refers to a range of wavelengths between 650–900 nm in which tissue absorbance and scattering are reduced relative to other wavelengths [24]. Optical imaging techniques typically operate in this range to maximize resolution, contrast, and penetration depths. The optical properties of tissue that govern these parameters, primarily absorption and scattering, vary across tissue types; therefore, the investigation of these properties preceded imaging applications. Furthermore, they are relevant to both photoacoustic imaging and optical coherence tomography—another modality has seen recent growth in oral diagnostic research.

Initial work focused on understanding the absorption and scattering properties of NIR light in healthy and carious/demineralized enamel [25–27]. For many years, dental caries have been diagnosed with visual, tactile, and radiographic exams; however, a significant level of variation exists across examiners. Healthy enamel is primarily composed of hydroxyapatite $(Ca_{10}(PO_4)_6(OH)_2)$ and is highly transparent to NIR light (Fig. 11.1a). During demineralization and decay, individual mineral crystals dissolve which causes micropores to form in carious lesions [28].
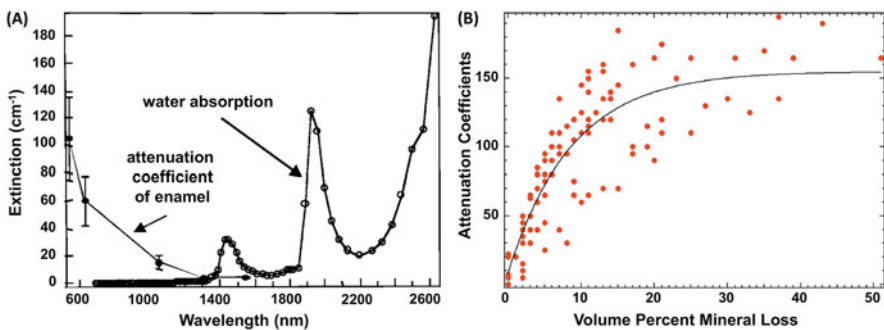

Fig. 11.1 Optical properties of enamel. (**a**) Plot of the attenuation coefficient of dental enamel versus the absorption profile of water in the NIR. (**b**) The attenuation coefficient has an exponential relationship ($r^2 = 0.74$) to the extent of mineral loss in enamel caries lesions. Adapted with permission from the Society of Photo-Optical Instrumentation Engineers [25]
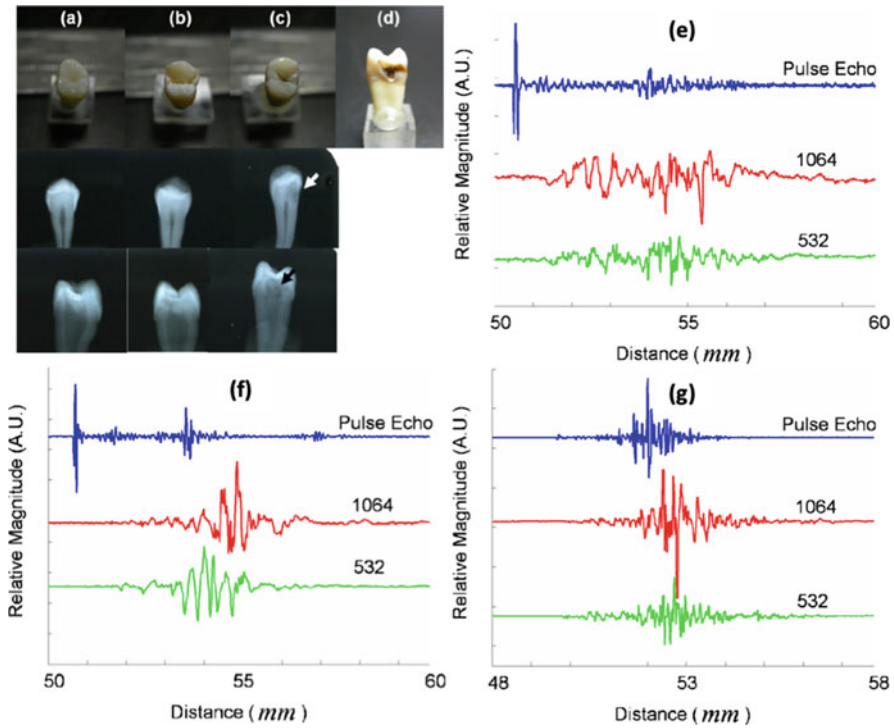
Fig. 11.2 Characterization of upper premolar health status through visual, radiographic, and photoacoustic indicators. The top row of photographs shows occlusal views of (**a**) healthy tooth, (**b**) incipient caries, (**c**) advanced caries, and (**d**) advanced from a proximal view, revealing penetration through the dentin. The lower radiographs show buccolingual views (second row) and proximal views (third row) of the same teeth—they exhibit low contrast from the caries. Pulse-echo and photoacoustic A-line signals are shown at 1064 nm and 532 nm for (**e**) healthy tooth, (**f**) incipient caries, and (**g**) advanced caries. Adapted with permission from the Society of Photo-Optical Instrumentation Engineers [34]

These pores strongly scatter visible and NIR light (Fig. 11.2b) [29]. Darling et al. found that the porosity of these lesions increased the scattering coefficient one to two orders of magnitude above healthy enamel. Indeed, the interactions of NIR light with enamel are dominated by scattering rather than absorption making absorption properties difficult to measure using optical methods [30]. Nevertheless, because photoacoustic intensity is proportional to optical absorption, photoacoustic ultrasound can measure relative absorption coefficients as well as true values if the light fluence is known quantitatively [31].

One of the earliest studies of photoacoustics for dentistry used a pulsed Nd:YAG (neodymium-doped yttrium aluminum garnet) laser to study the absorption and ablation properties of 1064 nm light on dentin and enamel [30]. The authors found that enamel absorbs poorly at 1064 nm so the photoacoustic signal is low. However, it increases with caries due to the presence of melanin from pigmented anaerobic

bacteria and their metabolites. In addition, the pulsed laser could be used for ablation of caries lesions, which could be monitored due to the higher photoacoustic signal from ablation (rapid expansion of vaporized organic material) compared to non-pigmented tissue. The acoustic properties of teeth following laser irradiation have also been studied to elucidate the acoustic differences between healthy and decayed teeth. El-Sharkawy et al. used an interferometric detection scheme for measuring surface acoustic waves, which propagate parallel to surfaces of irradiated teeth [32, 33]. The system could differentiate healthy and decayed teeth by calculating the longitudinal speed of sound, optical penetration depth, and Gruneisen coefficient for each sample—this photoacoustic spectroscopy scheme suggests the potential of automated caries diagnosis if used with pattern recognition algorithms. In 2006, Kim et al. extended the concept of detecting early-stage caries using photoacoustics [34]. They used a Nd:YAG laser (15-ns pulse width at 100 mJ, 10 Hz, 1064/532 nm) and an unfocused single element transducer (12 MHz) to analyze extracted human molars split into three groups (healthy, incipient caries, and advanced caries) as determined visually and radiographically. Here, incipient caries only affected the enamel, while advanced caries penetrated to the dentin. They found that the photoacoustic signal at 1064 nm was significantly stronger from regions of teeth with incipient caries than normal regions. This signal was further elevated for teeth with advanced caries. There was elevated signal between regions of teeth with incipient caries and normal teeth at 532 nm; importantly, the signal did not increase for advanced caries. This work was an important proof-of-concept but full photoacoustic imaging was not possible because the data acquisition was limited to one-dimension, i.e., only spectroscopic data.

11.3   Dentin and Enamel Imaging for Caries and Crack Detection

The photoacoustic technique was extended for imaging of dental caries in 2D and 3D in 2010 by Li et al. [35, 36]. They used a Q-Switched Nd:YAG laser (8-ns pulse width at 6 mJ, 2 Hz, 1064 nm) with a needle hydrophone aligned with an optical fiber for acoustic transduction. To acquire images, the probe was raster scanned using step motors. They also performed temperature and pressure field simulations in teeth to validate the safety of laser excitation. The 2D finite element modeling results suggested that the maximum local temperature change would be below $1\,^{\circ}C$ (where $\geq 5\,^{\circ}C$ is required for pulpal necrosis). In addition, the modeled pressure change in the dentin was <0.7 MPa, much less than its fatigue limit of 20 MPa. The authors could image both an extracted healthy tooth and one with caries (Fig. 11.3).

Photoacoustic tomography has been further investigated for early detection of dental lesions [37, 38]. Cheng et al. used a similar imaging system (8-ns pulse width, 10 Hz, 11 mJ/cm^2, 532 nm with 4.39 MHz ultrasound center frequency) to study extracted teeth with white spot enamel caries and artificially induced cracks. They used both typical B-mode photoacoustic tomography (contrast is proportional to the relative optical absorption in tissue) and "S-mode" tomography (where contrast is
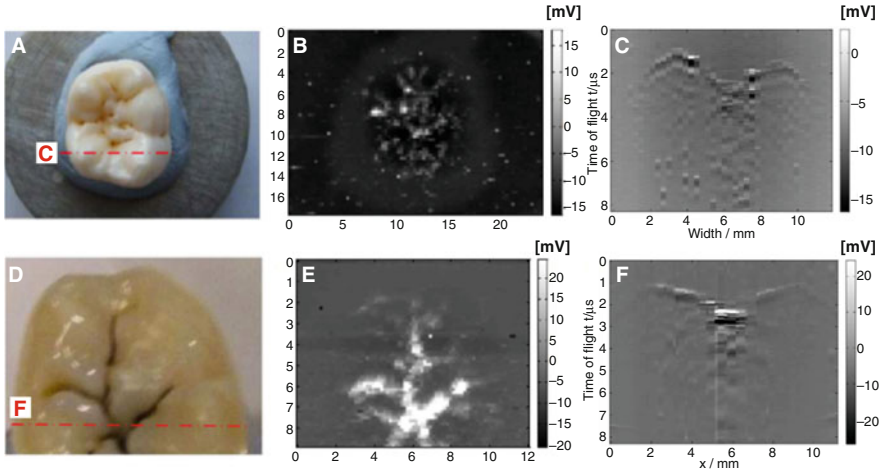
Fig. 11.3 Photoacoustic tomography of healthy versus carious teeth. (**a**) Occlusal photograph of a healthy extracted tooth. (**b**) Top-down (C-scan) photoacoustic image of the healthy tooth. (**c**) B-scan photoacoustic cross-section of a healthy tooth taken at the red line shown in Panel **a**. (**d**) Occlusal photograph of an extracted tooth with caries. (**e**) Top-down (C-scan) photoacoustic image of the diseased tooth. (**f**) B-scan photoacoustic cross-section of the diseased tooth at the red line shown in Panel **d**. Adapted with permission from the Institute of Physics [36]

determined by the spectral slope of the photoacoustic signal). This S-mode exploits the spectral profile of the photoacoustic echo rather than just its time-domain properties; it has shown potential for better differentiation of tissue types based on physical properties (such as the Young's modulus) than conventional photoacoustic imaging [39]. These authors found that the conventional B-mode technique was useful for imaging the structure of teeth including the enamel, dentin, and pulp. However, their images could not distinguish early enamel lesions. This limitation was primarily attributed to insufficient changes in optical absorption. Nevertheless, S-mode imaging could correlate differences in photoacoustic spectral slope to differences in stiffness between enamel and dentin as well as early enamel lesions. Rao et al. improved the resolution and contrast of these techniques with photoacoustic microscopy [40]. Photoacoustic microscopy is a form of photoacoustic imaging that can drastically improve resolution by using lenses to focus the excitation light analogous to traditional optical microscopy. There are two primary forms, and they are classified by the property that limits resolution: optical-resolution photoacoustic microscopy (OR-PAM) and acoustic-resolution photoacoustic microscopy (AR-PAM). In OR-PAM, the optical excitation and acoustic detection (single element ultrasound transducer) are co-focused to create dual foci that increase sensitivity. OR-PAM can generally achieve 0.5–3.0 μm resolutions with imaging depths of 1.2 mm. In AR-PAM, a cone of light is used for dark-field excitation of tissue and offers ∼45 μm resolutions with 5 mm imaging depths. Both of these modalities have been used to image extracted teeth. The authors found that the darkened
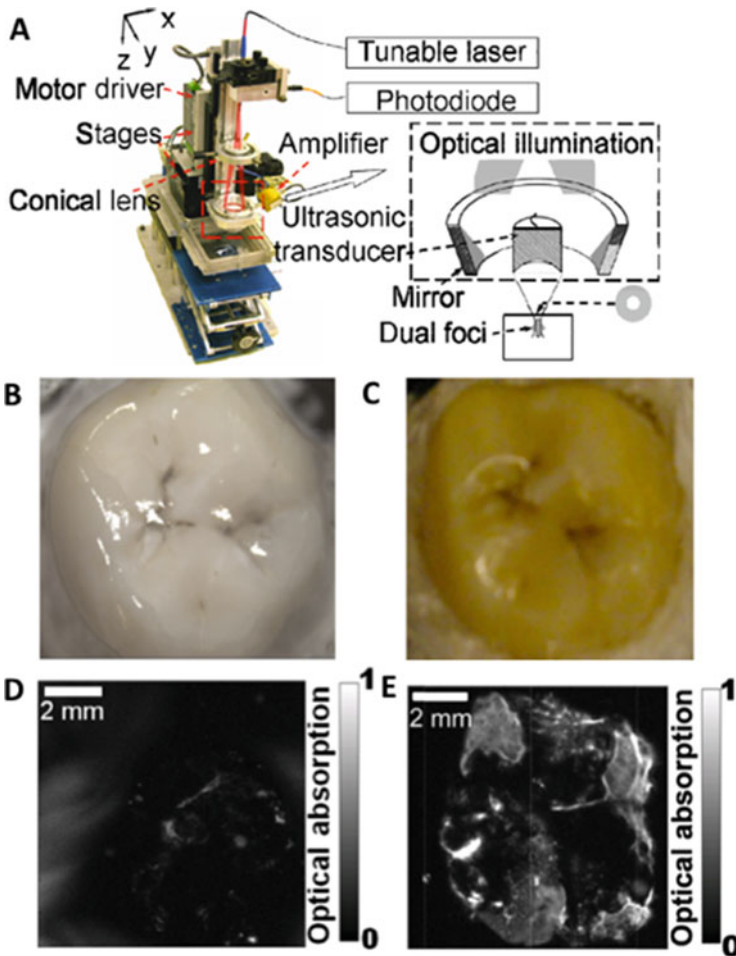
Fig. 11.4 Photoacoustic microscopy of healthy and decayed teeth. (**a**) Schematic of the AR-PAM hardware. (**b**) Occlusal photograph of a healthy extracted tooth and (**c**) a decaying extracted tooth. (**d**) AR-PAM image of the healthy tooth and (**e**) the decaying tooth. These images show significantly elevated optical absorption in the decayed tooth due to the pigmentation associated with dental lesions. Adapted with permission from the Society of Photo-Optical Instrumentation Engineers [40]

color characteristic of dental decay was correlated with increased photoacoustic intensity. Furthermore, healthy vs. decayed teeth showed significantly different intensities under AR-PAM (Fig. 11.4); of course, longitudinal tracking would be required to reliably quantify the progression of dental decay. One challenge noted by Periyasamy et al. is that photoacoustic signal from metal fillings can dominate the signal generated by the tooth itself introducing undesirable background when looking for dental lesions [41].

Hughes et al. also utilized photoacoustic microscopy in an all-optical configuration for early-stage detection of dental caries [42]. They showed that the optically generated ultrasonic signal in one-dimension alone could differentiate pre-caries lesions from healthy enamel; in addition, the sample could be scanned to acquire depth-resolved images revealing the extent of the sub-surface lesion (confirmed with histology). The authors noted that error in the measurement of enamel lesion thickness was about 3%, which they attributed to variation in the speed of sound caused by the lesions themselves. A larger error (30%) was present when measurements were made closer to the enamel dentine junction possibly due to the higher depth. Perhaps the largest limitation of photoacoustic microscopy is that it is not suited for in vivo imaging. To this end, a handheld PAM probe was recently reported, but it has not yet been demonstrated for dental applications [43].

11.4 Imaging Dental Pulp, Implants, and Periodontal Features

Accurate assessment of the pulp status is critical for the diagnosis of a number of conditions such as reversible/irreversible pulpitis, acute/chronic abscess, and necrosis. However, the objective measurement and characterization of pulp vitality remain a significant challenge in dental practice. The clinical gold standard is to perform sensitivity tests: these primarily refer to thermal testing (assessment of the response to hot and cold stimuli) and electric pulp testing, which is used to assess the status of pulpal nerve fibers. Unfortunately, these techniques are painful for the patient and do not necessarily reflect the status of the vascular supply. An ideal diagnostic tool would supply an objective, reproducible, non-painful, and accurate method for quantifying the vascular supply of a tooth. Some optical techniques such as pulse oximetry and laser Doppler flowmetry have been applied to probing pulpal blood oxygen saturation; however, these are primarily limited by the high scattering and absorption coefficients of the surrounding hard dental tissues. Yamada et al. conducted an early feasibility study on photoacoustic imaging of dental pulp in 2016 [44]. They investigated both 532 nm and 1064 nm wavelengths (100 Hz repetition rate, 1.2 ns pulsewidth, 1 mJ pulse energy, 4.6 MHz central frequency) for imaging extracted teeth. First, they imaged teeth split in half. In the first case, the root canal was filled with water and in the second case it was filled with 3% hemoglobin solution. At 532 nm, the water and the hemoglobin-filled samples could not be distinguished, primarily due to the strong scattering by the enamel and dentin. However, at 1064 nm, high frequency vibrations could be detected in the photoacoustic waveform of the hemoglobin-filled tooth that were not present in the water-filled tooth. Furthermore, the intensity of the high frequency signals had a linear correlation to the hemoglobin concentration. Unfortunately, the differences in frequency spectra between hemoglobin and water-filled whole teeth were much less significant than in split teeth. Photoacoustic imaging for diagnosis of pulp vitality is an attractive concept but is still largely unexplored. The intense reflection, scattering, and absorption of dentin and enamel will pose the largest challenge going forward. Another interesting application is in implant dentistry. Ultrasound

has recently been growing as a promising tool for evaluating implant status across multiple stages of treatment, and we recommend a recent review for a systematic discussion of this topic [1]. One of its limitations, however, is the lack of molecular contrast, which can be desirable for diagnosis and quantification of peri-implantitis. Peri-implantitis is an umbrella term for "destructive inflammatory processes around osseointegrated implants" that contribute to pocket deepening and crestal/alveolar bone loss [45, 46]. Lee et al. conducted initial work on this topic with photoacoustic imaging using porcine jaws ex vivo [47, 48]. They used a 532/1064 nm Q-switched Nd:YAG laser with a tunable (680–950 nm) OPO laser at 17.7 mJ/cm^2 for excitation with both an AR-PAM system (5 MHz central frequency) and a commercial US system (3–12 MHz central frequency) for detection. They then imaged a titanium implant with abutment and fixture both under chicken breast of varying thickness (10–20 mm) and after implantation at the site of the molar in an extracted porcine jawbone (Fig. 11.5). The authors found that the structure of the jawbone and internal position of the implant could be easily visualized with both systems. Of course, the entire bone structure could not be resolved as in radiographic techniques because the optical illumination and ultrasonic emission cannot penetrate through bone like X-rays. Nevertheless, they could determine the angle and length of the position under the jawbone in addition to the depth of the layer of soft tissue above it.

Finally, resolving the periodontal anatomy, especially the pocket depth, is of significant interest to clinical practice. Periodontal disease is currently and has historically been diagnosed by a combination of factors: pocket (probing) depth, attachment loss, mobility, bone loss, and degree of inflammation. The periodontal probe is often used for physically measuring the extent of apical epithelial attachment relative to the gingival margin. However, it is a highly variable technique that is time consuming and uncomfortable for patients; furthermore, the threads of dental implants often impede the physical probe measurements [49]. A facile imaging technique could potentially address these issues and improve the poor clinical rate of pocket depth charting [50, 51]. Optical coherence tomography is one option that has recently been explored for imaging the gingiva and periodontal structures in high resolution [52, 53]. This technique can resolve tissue microstructures and capillary vasculature with impressive detail, but unfortunately is limited to penetration depths of 2 mm due to optical tissue scattering. Though photoacoustic ultrasound cannot significantly improve the penetration depth through hard tissues, it can penetrate through centimeters of soft tissue (e.g. gingiva) because even diffuse photons can generate acoustic waves.

Our group has recently leveraged this ability for imaging the periodontal pocket in both swine jaws ex vivo [54] and the human mouth in vivo [55]. This work used a commercial, tomographic photoacoustic ultrasound system (16–40 MHz central frequency, 680–970 nm, 5-ns pulse width at 20 Hz) along with a food-grade contrast agent derived from cuttlefish ink. The spatial resolution of this system was roughly 300 μm in the photoacoustic mode and 100 μm in the ultrasound-only mode. The contrast agent contained melanin nanoparticles with broad absorption in the NIR and was used to irrigate the gingival sulcus using a micropipette tip or oral gavage, thereby enabling visualization of the pocket with photoacoustics. This contrast
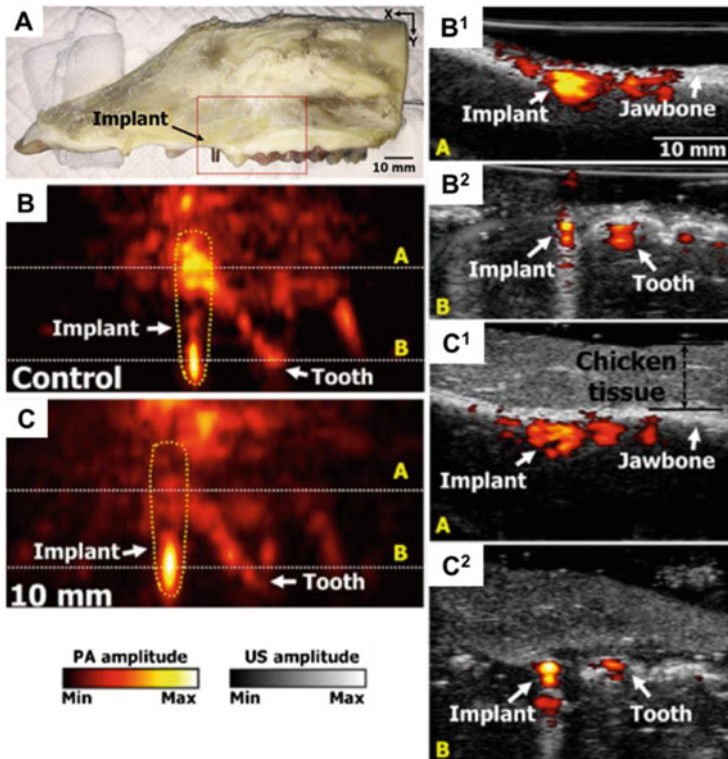
Fig. 11.5 Ex vivo imaging of a dental implant in a porcine jawbone using a clinical photo-acoustic/ultrasound tomography system. (**a**) Photograph of the porcine jawbone with implant. (**b**) Photoacoustic maximum amplitude projection of the titanium implant in the jawbone where (**b1**) and (**b2**) correspond to cross-sections of the dashed region in (**a**). (**c**) Photoacoustic maximum amplitude projection of the implant at the same location, under 10 mm of chicken breast tissue. (**c1**) and (**c2**) correspond to the dashed region in (**c**). Adapted with permission from The Optical Society [48]

media was chosen for its broad NIR absorbance, food-grade biocompatibility, and simple formulation. The technique was first conducted on 39 porcine teeth in extracted swine jaws, both with natural and artificially deepened pockets, and was validated with the conventional Williams probe (bias values $< \pm 0.25$ mm, $< 11\%$ variance) (Fig. 11.6). Shallow (1.65 mm), intermediate (2.04 mm), deep (4.45 mm), and artificially deep pockets (4.60 mm) were successfully measured. The ultrasound mode was also leveraged to measure 45 gingival thicknesses and compared to measurement with a needle. These measurements were only 0.07 mm larger than invasive examination. This bias could potentially be accounted for by the pressure generated by the needle during physical measurement. The contrast agent was also easily removed following rinsing with water (applied via a 5-mL syringe without needle) and normal tooth brushing.
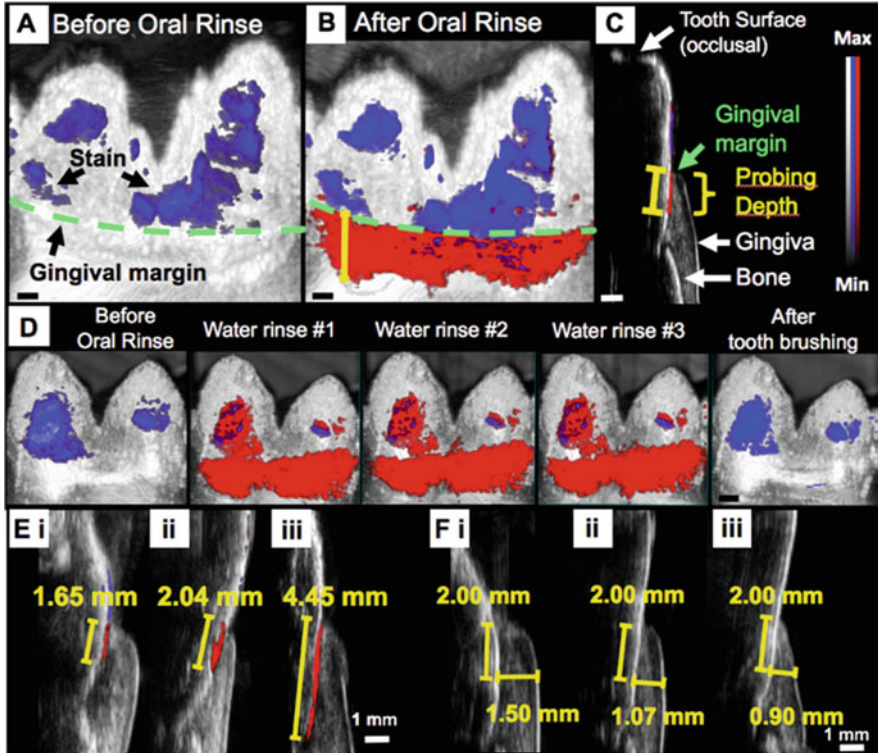
Fig. 11.6 Photoacoustic ultrasound images of swine molars using a food-grade contrast agent. (**a**) A mandibular molar prior to the administration of contrast using 680-nm excitation. Ultrasound signal is in grayscale while photoacoustic is in color; the blue signal is from tartar/calculus on the enamel. The green line shows the gingival margin. (**b**) The same tooth following irrigation of the pocket with contrast agent, shown in red. Differentiation between stain and contrast agent is possible by using both 680 and 800 nm excitation, due to their different absorption peaks. The red region reveals the pocket geometry and the probing depth for an arbitrary plane is shown with a yellow bar. (**c**) A sagittal plane from the 3D scan in (**b**) reveals the probing depth for that particular plane. The occlusal tooth surface, gingival margin, probing depth, gingiva, and bone are easily distinguished. Panel (**d**) shows the stability of labeling and the removal of the label with a toothbrush. The contrast agent remained in the pocket for multiple water rinses but was easily removed with brushing. (**e**) Representative sagittal images of a range of probing depths including 1.65 mm, 2.04 mm, and 4.45 mm. (**f**) Representative gingival thickness measurements taken 2.00 mm from the gingival margin with thicknesses of 1.50 mm, 1.07 mm, and 0.90 mm from different swine [54]

Subsequently, this application was extended to a case study in a healthy adult subject (Fig. 11.7). The relative standard deviation of five replicate measurements for a mandibular incisor was 10%. The depths measured by imaging agreed with conventional probing. Of note, all measurements were ≤2 mm because the imaging site was healthy incisors. One of the benefits of this approach was that the whole pocket could be mapped as opposed to single positions (e.g. mesiobuccal, central
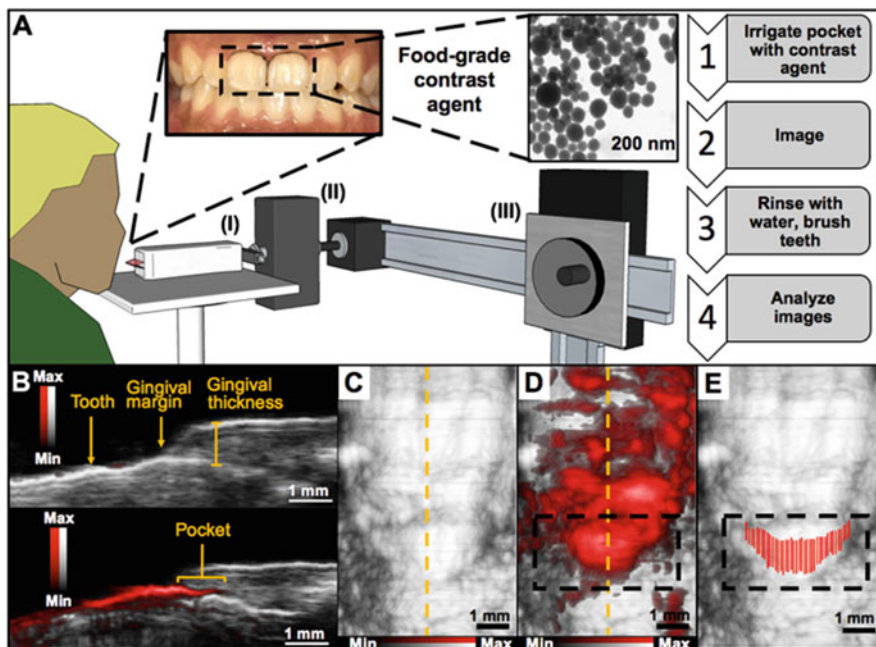
Fig. 11.7 Human data of photoacoustic ultrasound for pocket depth mapping. (**a**) Schematic of the imaging setup and workflow. The subject was scanned in an upright position by a photoacoustic ultrasound transducer (i) attached to a stepper motor (ii) and sliding frame (iii) for 3D imaging and positioning, respectively. Ultrasound gel was used for coupling. (**b**) A cross-section in the sagittal plane of a mandibular incisor at a central buccal position (yellow dashed line in **c**, **d**) showing the gingival margin before (top) and after (bottom) irrigation with contrast agent. The pocket depth was measured from the gingival margin to the edge of photoacoustic signal. The same incisor is shown in the frontal plane before (**c**) and after (**d**) irrigation. (**e**) The shape of the pocket could be reconstructed by measuring the pocket depth for each sagittal plane in the frontal image (~0.076 mm spacing) and overlaying these measurements onto the ultrasound-only image to remove nonspecific signal from the tooth and gingival surfaces [55]

buccal, and distobuccal) at a time. Additionally, the contrast agent was easily removed by rinsing with water and brushing the teeth as in the ex vivo porcine model. Current efforts are focused on streamlining the post-processing steps and miniaturizing the imaging hardware for improved access to distal teeth.

11.5   Outlook and Practical Considerations

One of the main advantages of ultrasound for dentistry is its ability to image the gingiva, which is mostly transparent to the common dental imaging modalities such as X-ray and cone beam computed tomography. In addition, it can resolve the surfaces and contours of hard tissues (e.g. tooth, bone) and integrate these

with the depth-resolved data from the gingiva. It follows, however, that the major limitations are its relative inability to image through tooth/bone and its limited grayscale contrast. Photoacoustic imaging can help overcome these limitations by shifting the contrast mechanism to the absorption of light rather than differences in refractive index, and extending penetration depths from the ballistic to the diffusive regime. Nevertheless, research to date suggests that photoacoustic analysis of teeth alone will probably be restricted to their surfaces (enamel and cementum).

Currently, a handful of practical challenges face the translation of photoacoustics to dentistry but we believe these are largely solvable. One example is the form factor of existing photoacoustic hardware. Most research-grade systems are meant for general purpose applications and utilize relatively large transducers that can only access the anterior teeth. Furthermore, the laser is housed separately. However, new hardware can be envisioned for the specific purpose of imaging within the oral cavity. These designs could potentially take the form of a mouthpiece transducer with coupled optical excitation or a handheld "hockey-stick" transducer for reaching the posterior teeth [56]. Another consideration for eventual clinical adoption is the price: Ultrasound is an inexpensive technique but the laser associated with photoacoustic imaging raises the cost significantly. It is possible, however, for systems to harness LED excitation sources that drastically reduce both the cost and overall footprint [57].

When taking 3D scans with a linear array transducer, it is necessary for the head of the subject to remain still. Otherwise, artifacts from minor movements will distort the final image. To combat this, a clinical setup would likely use a head immobilizer similar to those used for dental radiographs. Post-processing algorithms can also be employed to minimize these effects. Furthermore, since ultrasound waves do not propagate through air, the choice of coupling agent between oral surfaces and the transducer requires some consideration. Ultrasound gel is functional but requires re-sterilization of the transducer between patients in a clinical setting. Single-use materials for dry coupling may be useful in this context.

Photoacoustic imaging is a young technology but is developing at a rapid pace due to its optical contrast, good spatial resolution, and real-time imaging. Dental-specific investigations are still in their very early stages, but they show potential for caries detection, analysis of tooth surface integrity (crack detection), implant imaging, and characterization of the periodontium. With the growing availability of commercial photoacoustic systems, and the prevalence of custom preclinical systems, it is likely that photoacoustic imaging will continue to complement the developments in ultrasound techniques for dental applications.

References

1. Bhaskar V, et al. Updates on ultrasound research in implant dentistry: a systematic review of potential clinical indications. Dentomaxillofac Radiol. 2018;47(6):20180076. ISSN:0250-832X.

 2. David CM, Tiwari R. Ultrasound in maxillofacial imaging: a review. J Med Rad Pathol Surg. 2015;1(4):17–23. ISSN:2395-2075.
 3. Evirgen Ş, Kamburoğlu K. Review on the applications of ultrasonography in dentomaxillofacial region. World J Radiol. 2016;8(1):50.
 4. Hall A, Girkin JM. A review of potential new diagnostic modalities for caries lesions. J Dental Res. 2004;83 Suppl 1:89–94. ISSN:0022-0345.
 5. Kocasarac HD, Angelopoulos C. Ultrasound in dentistry: toward a future of radiation-free imaging. Dent Clin N Am. 2018;62(3):481–89. ISSN:0011-8532.
 6. Musu D, et al. Ultrasonography in the diagnosis of bone lesions of the jaws: a systematic review. Oral Surg Oral Med Oral Pathol Oral Radiol. 2016;122(1):e19–e29. ISSN:2212-4403.
 7. Sharma S, et al. Ultrasound as a diagnostic boon in Dentistry a review. Int J Sci Stud. 2014;2:2.
 8. Singh GP, Dogra S, Kumari E. Ultrasonography: maxillofacial applications. Ann Dent Spec 2014;2(3):104–7.
 9. Marotti J, et al. Recent advances of ultrasound imaging in dentistry – a review of the literature. Oral Surg Oral Med Oral Pathol Oral Radiol. 2013;115(6):819–32. ISSN:2212-4403. https://doi.org/10.1016/j.oooo.2013.03.012. http://www.sciencedirect.com/science/article/pii/S2212440313001727%20https://ac.els.cdn.com/S2212440313001727/.1.s2.0-S2212440313001727-main.pdf?_tid=7f0abd15-9b8b-4118-8d81-69e9a69c3eda&acdnat=1550271867_b0e72fb1058ebf78347938676ee6c2fb.
10. Zhou Y, Yao J, Wang LV. Tutorial on photoacoustic tomography. J Biomed Opt. 2016;21(6):1–14, 14. https://doi.org/10.1117/1.JBO.21.6.061007.
11. Wang LV, Hu S. Photoacoustic tomography: in vivo imaging from organelles to organs. Science. 2012;335(6075):1458–62. ISSN:0036-8075.
12. Xu M, Wang LV. Photoacoustic imaging in biomedicine. Rev Sci Instrum. 2006;77(4):041101. ISSN:0034-6748.
13. Rich LJ, Seshadri M. Photoacoustic imaging of vascular hemodynamics: validation with blood oxygenation level-dependent MR imaging. Radiology 2014;275(1):110–18. ISSN:0033-8419.
14. Hariri A, et al. In vivo photoacoustic imaging of chorioretinal oxygen gradients. J Biomed Opt 2018;23(3):036005. ISSN:1083-3668.
15. Zhang HF, et al. Imaging of hemoglobin oxygen saturation variations in single vessels in vivo using photoacoustic microscopy. Appl Phys Lett. 2007;90(5):053901. ISSN:0003-6951.
16. Mallidi S, Luke GP, Emelianov S. Photoacoustic imaging in cancer detection, diagnosis, and treatment guidance. Trends Biotechnol. 2011;29(5):213–21. ISSN:0167-7799.
17. Mehrmohammadi M, et al. Photoacoustic imaging for cancer detection and staging. Curr Mol Imaging. 2013;2(1):89–105. ISSN:2211-5552.
18. Moore C, Jokerst JV. Strategies for image-guided therapy surgery and drug delivery using photoacoustic imaging. Theranostics 2019;9(6):1550–71. ISSN:1838-7640. https://doi.org/10.715/thno.32362. https://www.ncbi.nlm.nih.gov/pubmed/31037123%20https://www.ncbi.nlm.nih.gov/pmc/articles/PMC6485201/.
19. Borg RE, Rochford J. Molecular photoacoustic contrast agents: design principles & applications. Photochem Photobiol. 2018;94(6):1175–1209. ISSN:0031-8655. https://doi.org/10.1111/php.12967. https://onlinelibrary.wiley.com/doi/abs/10.1111/php.12967.
20. Lemaster JE, Jokerst JV. What is new in nanoparticle-based photoacoustic imaging? Wiley Interdiscip Rev Nanomed Nanobiotechnol. 2017;9(1). ISSN:1939-0041 1939-5116. https://doi.org/10.1002/wnan.1404. https://www.ncbi.nlm.nih.gov/pubmed/27038222%20https://www.ncbi.nlm.nih.gov/pmc/articles/PMC5045757/.
21. Swierczewska M, Lee S, Chen X. Inorganic nanoparticles for multimodal molecular imaging. Mol Imaging. 2011;10(1). https://doi.org/10.2310/7290.2011.00001. https://journals.sagepub.com/doi/abs/10.2310/7290.2011.00001.
22. Jiang Y, Pu K. Multimodal biophotonics of semiconducting polymer nanoparticles. Acc Chem Res 2018;51(8):1840–49. ISSN:0001-4842. https://doi.org/10.1021/acs.accounts.8b00242.
23. Jiang Y, Pu K. Advanced photoacoustic imaging applications of near-infrared absorbing organic nanoparticles. Small. 2017;13(30):1700710. ISSN:1613-6810. https://doi.org/10.1002/smll.201700710. https://onlinelibrary.wiley.com/doi/abs/10.1002/smll.201700710.

24. Weissleder R. A clearer vision for in vivo imaging. Nat Biotechnol. 2001;19:316. https://doi.org/10.1038/86684.

25. Darling CL, Huynh G, Fried D. Light scattering properties of natural and artificially demineralized dental enamel at 1310 nm. J Biomed Opt 2006;11(3):034023. ISSN:1083-3668.

26. Fried D, et al. Nature of light scattering in dental enamel and dentin at visible and near-infrared wavelengths. Appl Opt 1995;34(7):1278–85. ISSN:2155-3165.

27. Spitzer D, Ten Bosch JJ. The absorption and scattering of light in bovine and human dental enamel. Calcif Tiss Res 1975;17(2):129–37. ISSN:0008-0594.

28. Neel EAA, et al. Demineralization-remineralization dynamics in teeth and bone. Int J Nanomed 2016;11:4743–63. ISSN:1178-2013; 1176-9114. https://doi.org/10.2147/IJN.S107624. https://www.ncbi.nlm.nih.gov/pubmed/27695330%20https://www.ncbi.nlm.nih.gov/pmc/PMC5034904/.

29. Fried D, et al. Early caries imaging and monitoring with near-infrared light. Dental Clin N Am 2005;49(4):771–93. ISSN:0011-8532. https://doiorg/10.1016/j.cden.2005.05.008. http://www.sciencedirect.com/science/article/pii/S0011853205000352.

30. Harris DM, Fried D. Pulsed Nd:YAG laser selective ablation of surface enamel caries: I. Photoacoustic response and FTIR spectroscopy. In: BiOS 2000 the international symposium on biomedical optics. SPIE. Vol. 3910; 2000. https://doi.org/10.1117/12.380823.

31. Rajian JR, Carson PL, Wang X. Quantitative photoacoustic measurement of tissue optical absorption spectrum aided by an optical contrast agent. Opt Express 2009;17(6):4879–89. https://doi.org/10.1364/OE.17.004879. http://www.opticsexpress.org/abstract.cfm?URI=oe-17-6-4879.

32. El-Sharkawy YH, El Sherif AF. Photoacoustic diagnosis of human teeth using interferometric detection scheme. Opt Laser Technol 2012;44(5):1501–06. ISSN:0030-3992.

33. El-Sharkawy YH, et al. Diagnostic of human teeth using photoacoustic response. In: Lasers in dentistry XII. Vol. 6137. San Francisco: International Society for Optics and Photonics; 2006. p. 613701.

34. Kim K, et al. Early detection of dental caries using photoacoustics. In: Photons plus ultrasound: imaging and sensing 2006: the seventh conference on biomedical thermoacoustics, optoacoustics, and acousto-optics. Vol. 6086. San Francisco: International Society for Optics and Photonics; 2006. p. 60860G.

35. Li T, Dewhurst RJ. Photoacoustic non-destructive evaluation and imaging of caries in dental samples. In: AIP conference proceedings. Vol. 1211. New York: AIP; 2010. p. 1574–81. ISBN:0735407487.

36. Li T, Dewhurst RJ. Photoacoustic imaging in both soft and hard biological tissue. In: Journal of physics: conference series. Vol. 214. Bristol: IOP Publishing; 1999. p. 012028. ISBN:1742-6596.

37. Cheng R, et al. Noninvasive assessment of early dental lesion using a dual-contrast photoacoustic tomography. Sci Rep 2016;6:21798. https://www.nature.com/articles/srep21798#supplementary-information. https://doi.org/10.1038/srep21798%20https://www.ncbi.nlm.nih.gov/pmc/articles/PMC4763185/pdf/srep21798.pdf.

38. Koyama T, Kakino S, Matsuura Y. Photoacoustic imaging of hidden dental caries by using a fiber-based probing system. In: Biomedical imaging and sensing conference. Vol. 10251. Bellingham: International Society for Optics and Photonics; 2017. p. 1025119.

39. Wang S, et al. Theoretical and experimental study of spectral characteristics of the photoacoustic signal from stochastically distributed particles. IEEE Trans Ultrason Ferroelectr Freq Control 2015;62(7):1245–55. ISSN:0885-3010. https://doi.org/10.1109/TUFFC.2014.006806.

40. Rao B, et al. Photoacoustic microscopy of human teeth. In: Lasers in dentistry XVII. Vol. 7884. San Francisco: International Society for Optics and Photonics; 2011. p. 78840U.

41. Periyasamy V, Rangaraj M, Pramanik M. Photoacoustic imaging of teeth for dentine imaging and enamel characterization. In: Lasers in dentistry XXIV. Vol. 10473. San Francisco: International Society for Optics and Photonics; 2018. p. 1047309.

42. Hughes DA, et al. Imaging and detection of early stage dental caries with an all-optical photoacoustic microscope. In: Journal of Physics: Conference Series. Vol. 581. Bristol: IOP Publishing; 2015. p. 012002. ISBN:1742-6596.
43. Electronic Article. 2017/10// 2017. https://doi.org/10.1038/s41598-017-132243.
44. Yamada A, Kakino S, Matsuura Y. Detection of photoacoustic signals from blood in dental pulp. Opt Photon J 2016;6(09):229.
45. Mombelli A, Müller N, Cionca N. The epidemiology of peri-implantitis. Clin Oral Implants Res 2012;23(s6):67–76. ISSN:0905-7161. https://doi.org/10.1111/j.1600-0501.2012.02541.x. https://onlinelibrary.wiley.com/doi/abs/10.1111/j.16000-501.2012.02541.x.
46. Naveau A, et al. Etiology and measurement of peri-implant crestal bone loss (CBL). J Clin Med 2019;8(2):166. ISSN:2077-0383. https://www.mdpi.com/2077-0383/8/2/166.
47. Lee D, Park S, Kim C. Dual-modal photoacoustic and ultrasound imaging of dental implants. In: SPIE BiOS. SPIE. Vol. 10494; 2018. p. 5.
48. Lee D, et al. Photoacoustic imaging of dental implants in a porcine jawbone ex vivo. Opt Lett 2017;42(9):1760–63. ISSN:1539-4794.
49. Schou S, et al. Probing around implants and teeth with healthy or inflamed peri-implant mucosa/gingiva: a histologic comparison in cynomolgus monkeys (Macaca fascicularis). Clin Oral Implants Res 2002;13(2):113–26. ISSN:0905-7161.
50. McFall WT, et al. Presence of periodontal data in patient records of general practitioners. J Periodontol 1988;59(7):445–49. ISSN:1943-3670.
51. Cole A, McMichael A. Audit of dental practice record-keeping: a PCT-coordinated clinical audit by Worcestershire dentists. Prim Dent Care 2009;16(3):85–93. ISSN:1355-7610.
52. Fernandes LO, et al. In vivo assessment of periodontal structures and measurement of gingival sulcus with optical coherence tomography: a pilot study. J Biophoton 2017;10(6–7):862–69. ISSN:1864-063X. https://onlinelibrary.wiley.com/doi/pdf/10.1002/jbio.201600082.
53. Le NM, et al. A noninvasive imaging and measurement using optical coherence tomography angiography for the assessment of gingiva: an in vivo study. J Biophoton 2018;11(12):e201800242. ISSN:1864-063X. https://doi.org/10.1002/jbio.201800242. https://onlinelibrary.wiley.com/doi/abs/10.1002/jbio.201800242.
54. Lin CY, et al. Photoacoustic imaging for noninvasive periodontal probing depth measurements. J Dent Res 2018;97(1):23–30. ISSN:0022-0345. https://www.ncbi.nlm.nih.gov/pmc/articles/PMC5755810/pdf/10.1177_0022034517729820.pdf.
55. Moore C, et al. Photoacoustic imaging for monitoring periodontal health: a first human study. Photoacoustics 2018;12:67–74. ISSN:2213-5979. https://www.ncbi.nlm.nih.gov/pmc/articles/PMC6226559/pdf/main.pdf.
56. Pirotte T, Veyckemans F. Ultrasound-guided subclavian vein cannulation in infants and children: a novel approach. Br J Anaesth 2007;98(4):509–14. ISSN:1471-6771.
57. Hariri A, et al. The characterization of an economic and portable LED-based photoacoustic imaging system to facilitate molecular imaging. Photoacoustics 2018;9:10–20. ISSN:2213-5979.